Check for updates

Research Article

Advances in Mechanical Engineering

Advances in Mechanical Engineering
2016, Vol. 8(9) 1–11
© The Author(s) 2016
DOI: 10.1177/1687814016670803
aime.sagepub.com
SAGE

Multibody dynamic simulation and transient analysis of quay crane spreader and lifting mechanism

Arunas Andziulis[1], Tomas Eglynas[1,2], Marijonas Bogdevicius[2], Mindaugas Jusis[1] and Audrius Senulis[1]

Abstract

Nowadays, container shipment in the intermodal terminals is overloaded. The quay crane and its control system have to be properly prepared for rapid cargo reloading. The advanced control system may increase container loading efficiency due to the reduced transportation time. However, faster transportation demands higher safety. In this article, the authors performed multibody dynamics simulation of the container spreader and lifting mechanism by analyzing more advanced mathematical model of the quay crane. Trolley motion and cargo swing angle transient responses of the dynamic system were acquired and analyzed during model simulation. The main target of this research is to determine the system behavior during transients. The simulation results showed that the transients induced by startup of the vertical spreader travel affect the whole crane system in all the investigated cases. In addition, the influence of flexible cable causes additional oscillations of cargo and reciprocating trolley displacement. The simulation of the container spreader and lifting mechanism will help detect motion deviations of the quay crane in real time.

Keywords

Multibody dynamics, transients, simulation, mathematical modeling, quay crane

Date received: 1 July 2016; accepted: 30 August 2016

Academic Editor: Crinela Pislaru

General introduction

Risk of cargo transportation process and impact of crane restrictions

Every year, container shipment is increasing and the container terminals get loaded more. Because of this situation, the terminals must load more containers using the same transportation equipment. One of the most important aspects of cargo loading is operation safety which can decrease in overloaded terminals.[1–3] In order to ensure safety of the container during transportation, an optimal operational strategy[4,5] of a quay crane control has to be ensured. In addition, the restrictions and limitations of the intermodal quay crane have to be appropriately assessed performing numerical simulations of multibody dynamics and the transient processes.

One of the most researched cargo damage reasons in the past years is container swinging.[2,6,7] The main cause of the container and spreader swinging is the flexible steel cable connection between the spreader and trolley of the quay crane.[8] The container can produce swinging motion because of different container weights, wind gusts, and human actions. As a result, more time is required for the container shipment from point A to

[1]Marine Science and Technology Centre, Klaipeda University, Klaipeda, Lithuania
[2]Department of Transport Technological Equipment, Vilnius Gediminas Technical University, Vilnius, Lithuania

Corresponding author:
Tomas Eglynas, Marine Science and Technology Centre, Klaipeda University, Bijunu g. 17-206, LT-91225 Klaipeda, Lithuania.
Email: tmse@inbox.lt

Creative Commons CC-BY: This article is distributed under the terms of the Creative Commons Attribution 3.0 License (http://www.creativecommons.org/licenses/by/3.0/) which permits any use, reproduction and distribution of the work without further permission provided the original work is attributed as specified on the SAGE and Open Access pages (https://us.sagepub.com/en-us/nam/open-access-at-sage).

Figure 1. Quay crane in port of Rotterdam.

point B due to the container swinging reduction process. Moreover, due to unstable crane motions, there is a probability that the container can be damaged if the collision with the quay crane structures occurs. Because of high safety risks, the container crane operation mostly is suspended during strong winds.

The numerical simulations of multibody system dynamics enable to apply limitations for better investigation of container sway reasons. Therefore, applying a common set of limitations to all cranes would not be efficient. Most of the container terminals use quay cranes with specifications depending on their loading demands. Some of the main technical limitations of the quay crane are hoisting capacity, hoisting speeds of the spreader, trolley traveling speed, gantry traveling speed, traveling distances, boom hoisting time, wind speed, and power supply.[9]

The most active recent research area is modeling of crane dynamics to increase cargo safety. The main target of such research is to determine the system behavior in different conditions.[9–11] A dynamic model of a three-dimensional (3D) overhead gantry crane system motion is proposed by Ismail et al.[10] The Lagrangian method is used for calculations. The trolley position and swing angle responses of the dynamic system have been acquired and analyzed during system simulation. These results are suitable for the development of effective control algorithms for a double-pendulum gantry crane system. Jaafar et al.[9] presented the development of nonlinear gantry crane system model, and the factors affecting the performance in terms of input voltage, cable length, payload mass, and trolley mass were investigated. The simulation results had shown that system response is very sensitive to the variation in the parameters. This is the main reason for container swinging and safety issues. The results of this research are very beneficial for the development of control algorithms.

Most of the models related to dynamic control and safety problems represent only one side of the problem, such as a crane control system with a state simulator. For example, in Tomczyk et al.,[12] a dynamic model for solving problems of load operation and positioning under different wind disturbances is developed. Cha et al.[13] investigated problems involving floating crane and the dynamics model was developed to simulate the motion of the heavy cargo.

The most recent research results by Wu et al.,[14] and Qian et al.,[15] which addresses container sway problem, provide solutions related to the design of control algorithms dedicated to compensate or minimize the sway movement of the container. The presented solutions give positive results, although not all the container sway reasons were estimated. Therefore, by additionally estimating more reasons of container sway, these control algorithms could be made more efficient.

In this article, the dynamic model of a quay crane container spreader and lifting mechanism is presented. The proposed multibody system could also be used as a tool for solving multiple problems, such as wind disturbances, transportation trajectory, and predictive control. The developed multibody numerical model of a quay crane spreader and lifting mechanism is based on real quay crane (Figure 1) mechanical structure.

According to the analysis of the other research, the more sophisticated and accurate model is presented, which evaluates additional factors such as motor-induced vibrations, eight flexible cable system, transmission, and pulleys. The model is used for estimating the dynamics of the crane container spreader. It was developed using the parameters of manufactured prototype size, motor performance, lifting power, and so on. In addition, the authors developed motion equations of the crane systems and defined the initial parameters for system simulation. So in the next section, a dynamic

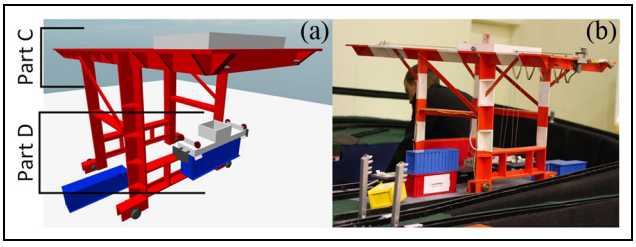

Figure 2. Scaled prototype of intermodal quay crane: (a) virtual prototype and (b) physical prototype.

model of container spreader dynamics and lifting mechanism is proposed.

Mathematical model and dynamics of container spreader transients

Before the development of better algorithm, a new mathematical model of the crane spreader and real quay crane prototype was created (Figure 2). The model will provide theoretical data about spreader status. The vibrations and their sources in the crane spreader and lifting mechanism were evaluated and provided additional information for new mathematical model for the crane (Figure 3). The mathematical model (Figure 3) marked "Part C" (trolley with lifting mechanism) and "Part D" (container spreader) is the same like in prototype (Figure 2).

Most attention is paid to motor vibrations and cable tensions. Because of very long cables in cranes, additional container swinging can appear. Mostly, it is caused by the weather conditions and wrong algorithms for operating devices. The best solution for this problem is adding additional sensors, such as, in our case, an accelerometer. The sensor's data could be used for containers' position estimation, detection, and reduction in container swinging. This could increase transportation security. Combined algorithm generator and real-time sensor data will provide the best algorithm for a particular kind of cargo that is stored in the container. In addition, it will allow adjusting algorithm in

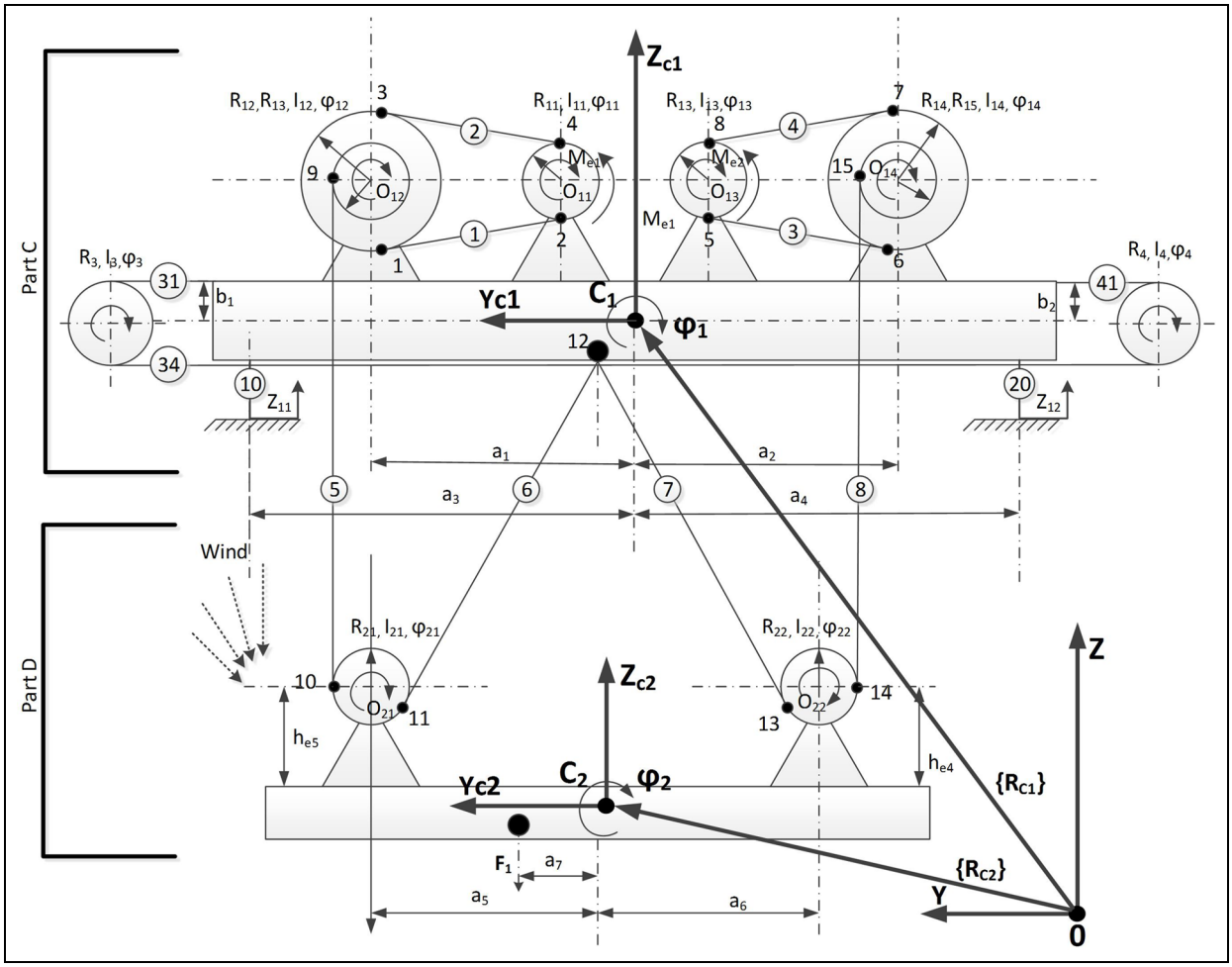

Figure 3. Dynamic model of quay crane spreader and lifting mechanism.

real time, if the weather conditions change or some unexpected situation appears (uneven control, shift of the cargo in the container, crane swinging due to the wind, etc.).

The developed model of the quay crane spreader and lifting mechanism is based on several assumptions. First, all bodies in the model are considered as solid bodies that cannot be deformed. The physical and mechanical properties of all the cables (such as stretching of cables while carrying heavy cargo) were assumed and estimated and their mathematical models are included in equations. Additionally, the electromechanical transient processes of electric motors and imperfections of trolley path were estimated.

For better container transportation problem solution, the new mathematical model was used for the container spreader and lifting mechanism, which will help to evaluate the situation. Torque mathematical equation of first electrical asynchronous motor with gear $\dot{M}_{ei}$ is shown below

$$\dot{M}_{ei} = U_{redei}C_{ei}(\omega_{ei0} - U_{redei}\dot{\varphi}_i) - d_{ei}M_{ei} \tag{1}$$

Here, d_{ei} and C_{ei} are the motor parameters, ω_{ei0} is the angular velocity, and U_{redei} is the gear ratio of the motor reduction. The analyzed system consists of two bodies with mass centers in points C_i and C_j. They are connected to the cable at mounting points i and j. The cable stiffness and damping coefficients are k_{ij} and c_{ij}, respectively. The tension force in this cable is F_{ij}, and the variation in mechanical work of this force is equal to

$$\delta W_{ij} = F_{ij}\delta L_{ij} \tag{2}$$

Here, L_{ij} is the distance between i and j; δL_{ij} is the variation in distance between i and j. The distance of L_{ij} is equal to

$$L_{ij}^2 = (\mathbf{r}_i - \mathbf{r}_j)^T(\mathbf{r}_i - \mathbf{r}_j) \tag{3}$$

Here, $\mathbf{r}_i$ and $\mathbf{r}_j$ are the vectors of i and j, respectively, in common coordinate system OXYZ

$$\begin{aligned}\mathbf{r}_i &= \mathbf{r}_{ci} + \mathbf{A}(\varphi_i)\mathbf{r}_{ci,i}\\ \mathbf{r}_j &= \mathbf{r}_{cj} + \mathbf{A}(\varphi_j)\mathbf{r}_{cj,j}\end{aligned} \tag{4}$$

Here, $\mathbf{r}_{Ci}$ and $\mathbf{r}_{Cj}$ are the vectors of mass centers of bodies, $\mathbf{A}(\varphi_i)$ and $\mathbf{A}(\varphi_j)$ are the matrixes of angular rotation (about X-axis), $\mathbf{r}_{ci,i}$ is the distance between body mass center C_i and body point i, and $\mathbf{r}_{cj,j}$ is the distance between body mass center C_j and body point j. The variation in distance L_{ij} is

$$\delta L_{ij} = \frac{\delta \mathbf{r}_{ij}^T}{L_{ij}}\mathbf{r}_{ij} \tag{5}$$

Here

$$\delta \mathbf{r}_{ij} = \delta \mathbf{r}_{ci} + \delta\varphi_i\left[\frac{d\mathbf{A}(\varphi_i)}{d\varphi_i}\right]\mathbf{r}_{ci,i} - \delta \mathbf{r}_{cj} - \delta\varphi_j\left[\frac{d\mathbf{A}(\varphi_j)}{d\varphi_j}\right]\mathbf{r}_{cj,j} \tag{6}$$

Using equations (5) and (6), the variations in mechanical work can be calculated as

$$\delta W_{cj} = \delta \mathbf{r}_{ci}^T \cdot \mathbf{q}_{r_{ci}} + \delta\varphi_i q_{r_i} + \delta \mathbf{r}_{cj}^T \mathbf{q}_{r_{cj}} + \delta\varphi_j q_{r_j} \tag{7}$$

Here, $\mathbf{q}_{r_{ci}}$ and $\mathbf{q}_{r_{cj}}$ are the vectors of the generalized forces that apply to bodies i and j; q_{r_i} and q_{r_j} are the generalized forces that apply to bodies i and j

$$\mathbf{q}_{r_{ci}} = \frac{F_{ij}}{L_{ij}}\mathbf{r}_{ij}, q_{\varphi i} = \frac{F_{ij}}{L_{ij}} r_{ci,i}^T\left[\frac{d\mathbf{A}(\varphi_i)}{d\varphi_i}\right]^T\mathbf{r}_{ij} \tag{8}$$

$$\mathbf{q}_{R_{cj}} = \frac{F_{ij}}{L_{ij}}\mathbf{r}_{ij}, q_{\varphi j} = \frac{F_{ij}}{L_{ij}}\mathbf{r}_{cj,j}^T\left[\frac{d\mathbf{A}(\varphi_j)}{d\varphi_j}\right]^T\mathbf{r}_{ij} \tag{9}$$

The cable tension force is

$$F_{ij} = \left(-k_{ij}(L_{ij} - L_{ij,0}) - C_{ij}\dot{L}_{ij}\right)H(L_{ij} - L_{ij,0}) \tag{10}$$

Here, $H(L_{ij} - L_{ij,0})$ is the Heaviside function and $L_{ij,0}$ is the initial cable length between i and j. $\dot{L}_{ij}$ is the cable linear speed

$$\dot{L}_{ij} = \frac{1}{L_{ij}}\dot{\mathbf{r}}_{ij}^T \cdot \mathbf{r}_{ij} \tag{11}$$

Here, $\dot{\mathbf{r}}_{ij}$ is the time derivative of vector $\mathbf{r}_{ij}$

$$\dot{\mathbf{r}}_{ij} = \dot{\mathbf{r}}_{ci} + \dot{\varphi}_i\left[\frac{d\mathbf{A}(\varphi_i)}{d\varphi_i}\right]\mathbf{r}_{ci,i} - \dot{\mathbf{r}}_{cj} - \dot{\varphi}_j\left[\frac{d\mathbf{A}(\varphi_j)}{d\varphi_j}\right]\mathbf{r}_{cj,j} \tag{12}$$

Equations of motions

System of motion equations for the first body (crane without load)

$$\begin{aligned}m_1\ddot{q}_{12} = &- k_{31}(q_{12} - R_3\varphi_3) - c_{31}(\dot{q}_{12} - R_3\dot{\varphi}_3)\\ &- k_{41}(q_{12} - R_3\varphi_4) - c_{41}(\dot{q}_{12} - R_4\dot{\varphi}_4)\\ &+ \mathbf{e}_2^T(F_5\mathbf{q}_{51} + F_6\mathbf{q}_{61} + F_7\mathbf{q}_{71} + F_8\mathbf{q}_{81})\\ &- \dot{m}_1\dot{q}_{12} + F_{1R2}\end{aligned} \tag{13}$$

$$\begin{aligned}m_1\ddot{q}_{13} = &- k_{10}(q_{13} + a_3\varphi_1 - \mathbf{Z}_{11})\\ &- k_{20}(q_{13} - a_4\varphi_1 - \mathbf{Z}_{12}) - c_{20}(\dot{q}_{13} - a_4\dot{\varphi}_1 - \mathbf{Z}_{12})\\ &- c_{10}(\dot{q}_{13} + a_3\dot{\varphi}_1 - \mathbf{Z}_{11}) - m_1 g - \dot{m}_1\dot{q}_{13}\\ &+ \mathbf{e}_3^T(F_5\mathbf{q}_{51} + F_6\mathbf{q}_{61} + F_7\mathbf{q}_{71} + F_8\mathbf{q}_{81}) + F_{1R3}\end{aligned} \tag{14}$$

$$\begin{aligned} I_1\ddot{\varphi}_1 = & -k_{10}a_3(q_{13} + a_3\varphi_1 - \mathbf{Z}_{11}) \\ & - c_{10}a_3(\dot{q}_{13} + a_3\dot{\varphi}_1 - \mathbf{Z}_{11}) \\ & - k_{20}a_4(q_{13} - a_4\varphi_1 - \mathbf{Z}_{12}) \\ & + c_{20}a_4(\dot{q}_{13} - a_4\dot{\varphi}_1 - \mathbf{Z}_{12}) - \dot{I}_1\dot{\varphi}_1 + M_{51} \\ & + M_{61} + M_{71} + M_{81} + M_{1\mathrm{R}} \end{aligned} \quad (15)$$

Here, m_1 is the mass of the first body, I_1 is the inertial moment of the first body about the X-axis, $\dot{m}_1$ and $\dot{I}_1$ are the first time derivatives of mass and mass inertial moment of the first body (assumption of cable winding on the pulley), respectively. a_3 and a_4 are the geometrical parameters. $\mathbf{Z}_{11}$ and $\mathbf{Z}_{12}$ are the kinematic excitations of the first body pulleys; $\mathbf{Z}_{11}$ and $\mathbf{Z}_{12}$ are the derivatives of kinematic excitations by time. $\mathbf{e}_2$ and $\mathbf{e}_3$ are the unit vectors on Y- and Z-axis in common coordinate system OXYZ. k_{31}, k_{41}, c_{31}, and c_{41} are stiffness and damping coefficients of trolley positioning system belts. k_{10}, k_{20}, c_{10}, and c_{20} are the stiffness and damping coefficients of the pulleys of trolley positioning system. F_5, F_6, F_7, and F_8 are the cable tension forces. M_{51}, M_{61}, M_{71}, M_{81}, and M_{1R} are the torques of the first body, transferred by cables 5, 6, 7, and 8. F_{1R2} and F_{1R3} are the air resistance forces (projection on Y- and Z-axis) and torques $\mathbf{q}_{51}$, $\mathbf{q}_{61}$, $\mathbf{q}_{71}$, and $\mathbf{q}_{81}$ are the vectors of the generalized forces of cables 5, 6, 7, and 8, respectively, determined using equation (8).

System of motion equations for the second body (spreader with the container)

$$\mathbf{M}_2\ddot{\mathbf{r}}_{C_2} = \mathbf{q}_{52} + \mathbf{q}_{62} + \mathbf{q}_{72} + \mathbf{q}_{82} + \mathbf{f}_{2W} + \mathbf{f}_{2R} \quad (16)$$

$$I_2\ddot{\varphi}_2 = M_{52} + M_{62} + M_{72} + M_{82} + M_{\mathrm{R2}} \quad (17)$$

$$I_{21}\ddot{\varphi}_{21} = R_{21}(F_5 - F_6) - M_{fr_{21}}sign(\dot{\varphi}_{21}) \quad (18)$$

$$I_{22}\ddot{\varphi}_{22} = R_{22}(F_7 - F_8) - M_{fr_{22}}sign(\dot{\varphi}_{22}) \quad (19)$$

Here, F_{2W} is the vector of weight force (20); $\mathbf{f}_{2R}$ and M_{R2} are the vector of air resistance force and torque of the second body, respectively. $\mathbf{q}_{52}$, $\mathbf{q}_{62}$, $\mathbf{q}_{72}$, and $\mathbf{q}_{82}$ are the vectors of the generalized forces of cables 5, 6, 7, and 8, respectively, calculated using equation (8). M_{52}, M_{62}, M_{72}, and M_{82} are the torques of the first body, transferred by cables 5, 6, 7, and 8, respectively. $\mathbf{M}_2$ is the matrix of masses of the second body calculated using equation (19). $M_{fr_{21}}$ and $M_{fr_{22}}$ are the torques of friction of polyspast

$$\{\boldsymbol{F}_{2W}\}^T = [0, 0, -m_2g] \quad (20)$$

$$[\boldsymbol{M}_2] = diag(m_2, m_2, I_2) \quad (21)$$

System of motion equations for the third and fourth bodies and the third asynchronous motor torque (trolley motion equations)

$$\dot{M}_{e3} = U_{rede3}C_{e3}(\omega_{e30} - U_{rede3}\dot{\varphi}_3) - d_{e3}M_{e3} \quad (22)$$

$$\begin{aligned} I_3\ddot{\varphi}_3 = & -k_{31}R_3(R_3\varphi_3 - q_{12}) - c_{31}R_3(R_3\dot{\varphi}_3 - \dot{q}_{12}) \\ & - k_{34}R_3(R_3\varphi_3 - R_4\varphi_4) - c_{34}R_3(R_3\dot{\varphi}_3 - R_4\dot{\varphi}_4) \\ & + M_{e3} - M_{e3R} \end{aligned} \quad (23)$$

$$\begin{aligned} I_4\ddot{\varphi}_4 = & -R_4k_{41}(R_4\varphi_4 - q_{12}) - R_4c_{41}(R_4\dot{\varphi}_4 - \dot{q}_{12}) \\ & - R_4k_{34}(R_4\varphi_4 - R_3\varphi_3) \\ & - R_4c_{34}(R_4\dot{\varphi}_4 - R_3\dot{\varphi}_3) - M_{e4R} \end{aligned} \quad (24)$$

Here, k_{31}, k_{34}, c_{31}, and c_{34} are the stiffness and damping coefficients of belts. φ_3, φ_4, $\dot{\varphi}_3$, and $\dot{\varphi}_4$ are the angular position and speed of the third and fourth bodies. R_3 and R_4 are the radii of the pulleys, I_3 is the mass moment of inertia of the third motor and pulley, and I_4 is the moment of inertia of the fourth pulley. M_{e3} is the torque of the motor. C_{e3} and d_{e3} are the motor parameters. M_{e3R} is the torque of resistance of the third body. ω_{e30} is the motor angular velocity.

System of motion equations for lifting mechanism

$$\dot{M}_{e1} = U_{rede1}C_{e1}(\omega_{e110} - U_{rede1}\dot{\varphi}_{11}) - d_{e1}M_{e1} \quad (25)$$

$$\begin{aligned} I_{11}\ddot{\varphi}_{11} = & -R_{11}(k_1(R_{11}\varphi_{11} - R_{12}\varphi_{12}) \\ & + c_1(R_{11}\dot{\varphi}_{11} - R_{12}\dot{\varphi}_{12}))(1 - e^{-f_{belt}\beta_{24}}) \\ & + M_{e1} - M_{fr_{11}}sign(\dot{\varphi}_{11}) \end{aligned} \quad (26)$$

$$\begin{aligned} I_{12}\ddot{\varphi}_{12} = & -R_{12}(k_1(R_{12}\varphi_{12} - R_{11}\varphi_{11}) \\ & + c_1(R_{12}\dot{\varphi}_{12} - R_{11}\dot{\varphi}_{11}))(1 - e^{-f_{belt}\beta_{13}}) \\ & - M_{9,5} - M_{fr_{12}}sign(\dot{\varphi}_{12}) \end{aligned} \quad (27)$$

$$\dot{M}_{e2} = U_{rede2}C_{e2}(\omega_{e130} - U_{rede2}\dot{\varphi}_{13}) - d_{e2}M_{e2} \quad (28)$$

$$\begin{aligned} I_{13}\ddot{\varphi}_{13} = & -R_{13}(k_3(R_{13}\varphi_{13} - R_{14}\varphi_{14}) \\ & + c_3(R_{13}\dot{\varphi}_{13} - R_{14}\dot{\varphi}_{14}))(1 - e^{-f_{belt}\beta_{58}}) \\ & + M_{e2} - M_{fr_{13}}sign(\dot{\varphi}_{13}) \end{aligned} \quad (29)$$

$$\begin{aligned} I_{14}\ddot{\varphi}_{14} = & -R_{14}(k_3(R_{14}\varphi_{14} - R_{13}\varphi_{13}) \\ & + c_3(R_{14}\dot{\varphi}_{14} - R_{13}\dot{\varphi}_{13}))(1 - e^{-f_{belt}\beta_{67}}) \\ & - M_{fr_{14}}sign(\dot{\varphi}_{14}) - M_{15,8} - M_{fr_{14}}sign(\dot{\varphi}_{14}) \end{aligned} \quad (30)$$

$$M_{9,5} = F_5R_{13}, M_{15,8} = F_8R_{14} \quad (31)$$

where M_{e1} and M_{e2} are the torques of the first and second asynchronous motors, respectively; φ_{11}, φ_{12}, φ_{13}, and φ_{14} are the angular positions of the first, second, third, and fourth pulleys, respectively. C_{e1}, d_{e1}, C_{e2}, and d_{e2} are the first and second motor parameters. ω_{e110} and ω_{e130} are the first and second motor angular velocities, respectively. I_{11}, I_{12}, I_{13}, and I_{14} are the moments of inertia of the first, second, third, and fourth pulleys,

respectively. R_{11}, R_{12}, R_{13}, and R_{14} are the radii of the first, second, third, and fourth pulleys, respectively. k_1, k_2, k_3, k_4, c_1, c_2, c_3, and c_4 are the stiffness and damping coefficients of the belts. $M_{9,5}$ and $M_{15,8}$ are the moments of inertia of the second and fourth pulleys, caused by the tension forces in cables 5 and 8, on points 9 and 15 of the pulleys, respectively. $M_{fr_{11}}$, $M_{fr_{12}}$, $M_{fr_{13}}$, and $M_{fr_{14}}$ are the torques of the friction force of the first, second, third, and fourth pulleys, respectively. f_{belt} is the friction coefficient; β_{24}, β_{13}, β_{58}, and β_{67} are the angles of belt warp.

System of equations for generalized forces of the fifth cable

$$\mathbf{q}_5 = \frac{F_5}{L_{9,10}}(\mathbf{r}_9 - \mathbf{r}_{10}) \tag{32}$$

$$F_5 = -k_5(L_{9,10} - L_{9,10,0}) - c_5\dot{L}_{9,10} \tag{32a}$$

$$\mathbf{r}_9 = \mathbf{r}_{C1} + \mathbf{A}_1(\varphi_1)\mathbf{r}_{C1,9} \tag{32b}$$

$$\mathbf{r}_{C1,9} = \mathbf{r}_{C1,O12} + \mathbf{r}_{O12,9} \tag{32c}$$

$$\mathbf{r}_{10} = \mathbf{r}_{C2} + \mathbf{A}_2(\varphi_2)(\mathbf{r}_{C2,O21} + \mathbf{r}_{O21,10}) \tag{32d}$$

$$\mathbf{r}_{9,10} = \mathbf{r}_9 - \mathbf{r}_{10} \tag{32e}$$

$$L_{9,10}^2 = \mathbf{r}_{9,10}{}^T\mathbf{r}_{9,10} \tag{32f}$$

$$\dot{L}_{9,10} = \frac{1}{L_{9,10}} - \dot{\mathbf{r}}_{9,10}{}^T\mathbf{r}_{9,10} \tag{32g}$$

$$\dot{\mathbf{r}}_{9,10} = \dot{\mathbf{r}}_9 - \dot{\mathbf{r}}_{10} \tag{32h}$$

$$\dot{\mathbf{r}}_9 = \dot{\mathbf{r}}_{C1} + \dot{\varphi}_1\left[\frac{d\mathbf{A}_1}{d\varphi_1}\right]\mathbf{r}_{C1,9} + \mathbf{A}_1(\varphi_1)\dot{\mathbf{r}}_{C1,9} \tag{32i}$$

$$\dot{\mathbf{r}}_{10} = \dot{\mathbf{r}}_{C2} + \dot{\varphi}_2\left[\frac{d\mathbf{A}_2}{d\varphi_2}\right]\mathbf{r}_{C2,10} + \mathbf{A}_2(\varphi_2)\dot{\mathbf{r}}_{C2,10} \tag{32j}$$

$$\dot{\mathbf{r}}_{10} = \dot{\mathbf{r}}_{C2} + \dot{\varphi}_2\left[\frac{d\mathbf{A}_2}{d\varphi_2}\right]\mathbf{r}_{C2,10} + \mathbf{A}_2(\varphi_2)\dot{\mathbf{r}}_{C2,10} \tag{32k}$$

$$\mathbf{r}_{O12,9} = \begin{Bmatrix} R_{13}\cos\beta_{9,10} \\ R_{13}\sin\beta_{9,10} \end{Bmatrix} \tag{32l}$$

$$\beta_{9,10} = \alpha_{O12,O21} - \gamma_{9,10} \tag{32m}$$

$$\sin\alpha_{O12,O21} = \frac{Y_{O21} - Y_{O12}}{L_{O12,O21}} \tag{32n}$$

$$\sin\gamma_{9,10} = \frac{R_{13} - R_{21}}{L_{O12,O21}} \tag{32o}$$

$$L_{O12,O21}^2 = (\mathbf{r}_{O12} - \mathbf{r}_{O21})^T(\mathbf{r}_{O12} - \mathbf{r}_{O21}) \tag{32p}$$

$$\mathbf{r}_{O21,10} = \begin{Bmatrix} R_{21}\cos\beta_{O11,O21} \\ R_{21}\sin\beta_{O11,O21} \end{Bmatrix} \tag{32q}$$

$$\mathbf{r}_{C2,10} = \mathbf{r}_{C2,O21} + \mathbf{r}_{O21,10} \tag{32r}$$

$$\mathbf{r}_{O21,10} = \begin{Bmatrix} R_{21}\cos\beta_{9,10} \\ R_{21}\cos\beta_{9,10} \end{Bmatrix} \tag{32s}$$

Here, k_5 and c_5 are the stiffness and damping coefficients of the fifth cable, respectively (k_5 depends on line length $L_{9,10}$). R_{21} is the radius of the left pulley on the trolley.

System of equations for generalized forces of the sixth, seventh, and eighth cables using system of equations (32)

$$\mathbf{q}_6 = \frac{F_6}{L_{11,12}}(\mathbf{r}_{12} - \mathbf{r}_{11}) \tag{33}$$

$$\mathbf{q}_7 = \frac{F_7}{L_{12,13}}(\mathbf{r}_{12} - \mathbf{r}_{13}) \tag{34}$$

$$\mathbf{q}_8 = \frac{F_8}{L_{14,15}}(\mathbf{r}_{14} - \mathbf{r}_{15}) \tag{35}$$

Moments applied on the first and second bodies

$$\begin{aligned}
M_{51} &= \mathbf{e}_x{}^T\left(\tilde{\mathbf{r}}_{C1,9}\cdot\mathbf{A}_1(\varphi_1)^T\cdot\mathbf{q}_5\right)\\
M_{61} &= \mathbf{e}_x{}^T\left(\tilde{\mathbf{r}}_{C1,12}\cdot\mathbf{A}_1(\varphi_1)^T\cdot\mathbf{q}_6\right)\\
M_{71} &= \mathbf{e}_x{}^T\left(\tilde{\mathbf{r}}_{C1,12}\cdot\mathbf{A}_1(\varphi_1)^T\cdot\mathbf{q}_7\right)\\
M_{81} &= \mathbf{e}_x{}^T\left(\tilde{\mathbf{r}}_{C1,15}\cdot\mathbf{A}_1(\varphi_1)^T\cdot\mathbf{q}_8\right)\\
M_{52} &= \mathbf{e}_x{}^T\left(\tilde{\mathbf{r}}_{C2,10}\cdot\mathbf{A}_2(\varphi_2)^T\cdot\mathbf{q}_5\right)\\
M_{62} &= \mathbf{e}_x{}^T\left(\tilde{\mathbf{r}}_{C2,11}\cdot\mathbf{A}_2(\varphi_2)^T\cdot\mathbf{q}_6\right)\\
M_{72} &= \mathbf{e}_x{}^T\left(\tilde{\mathbf{r}}_{C2,13}\cdot\mathbf{A}_2(\varphi_2)^T\cdot\mathbf{q}_7\right)\\
M_{82} &= \mathbf{e}_x{}^T\left(\tilde{\mathbf{r}}_{C2,14}\cdot\mathbf{A}_2(\varphi_2)^T\cdot\mathbf{q}_8\right)\\
M_{1\mathrm{R}} &= \mathbf{e}_x{}^T\left(\tilde{\mathbf{r}}_{C1p}\cdot\mathbf{A}_1(\varphi_1)^T\cdot\mathbf{f}_{1\mathrm{R}}\right)\\
M_{2\mathrm{R}} &= e_x{}^T\left(\tilde{\mathbf{r}}_{C2\mathrm{p}}\cdot\mathbf{A}_2(\varphi_2)^T\cdot\mathbf{f}_{2\mathrm{R}}\right)
\end{aligned} \tag{36}$$

Here, $\{e_x\}$ and $\{e_z\}$ are the unit vectors; $\{e_x\}^T = [1,0,0]$ and $\{e_z\}^T = [0,0,1]$. $[\tilde{r}_{Cl,k}]$ is the asymmetric matrix

$$\tilde{\mathbf{r}}_{Cl,k} = \begin{bmatrix} o & -r_{Cl,k\mathrm{Z}} & r_{Cl,k\mathrm{Y}} \\ r_{Cl,k\mathrm{Z}} & o & -r_{Cl,k\mathrm{X}} \\ -r_{Cl,k\mathrm{Y}} & r_{Cl,k\mathrm{X}} & o \end{bmatrix} \tag{37}$$

Here, $k = 9, 10, 11, 12, 13, 14, 15$ and $l = 1, 2$.

Equations of air resistances of the first and second bodies

$$\begin{aligned}
\mathbf{f}_{1R} = &-\left(\frac{1}{2}\rho_{air}A_{1\mathrm{R}}C_{1R}\dot{\mathbf{r}}_{C1}{}^T\dot{\mathbf{r}}_{C1}\right)\frac{\dot{\mathbf{r}}_{C2}}{[\dot{\mathbf{r}}_{C2}]}\\
&+\left(\frac{1}{2}\rho_{air}A_{1\mathrm{R}}C_{1R}\mathbf{v}_{wind}{}^T\mathbf{v}_{wind}\right)
\end{aligned} \tag{38}$$

Table 1. Initial values and model parameters used for the mathematical experiment.

System parameters	Units of measurement	Values	System parameters	Units of measurement	Values
a_1	m	0.062	R_{11}	m	0.02
a_2	M	0.1	R_{12}	m	0.04
a_3	m	0.2	R_{13}	m	0.02
a_4	m	0.2	R_{14}	m	0.02
a_5	m	0.1	R_{15}	m	0.04
a_6	M	0.1	R_{16}	m	0.02
I_1	kg m^2	10^{-3}	R_{21}	m	0.02
I_2	kg m^2	10^{-3}	R_{22}	m	0.02
I_{11}	kg m^2	10^{-4}	b_1	m	0.02
I_{12}	kg m^2	10^{-4}	b_2	m	0.02
I_{13}	kg m^2	10^{-4}	b_3	m	0.1
I_{14}	kg m^2	10^{-4}	b_4	m	0.1
I_3	kg m^2	10^{-3}	b_5	m	0.1
I_4	kg m^2	10^{-3}	b_6	m	0.1
I_{21}	kg m^2	10^{-4}	b_7	m	0.2
I_{22}	kg m^2	10^{-4}	m_{C1}	kg	1.872
C_{ei}	N m	379.12	m_{C2}	kg	0.765
d_{e1}	1/s	46.728	U_{red1}	–	20
k_x	N/m	106	U_{red2}	–	20
c_x	N s/m	0.01	Δt	s	10^{-5}

$$\mathbf{f}_{2R} = -\left(\frac{1}{2}\rho_{air}A_{2R}C_{2R}\dot{\mathbf{r}}_{C2}{}^{T}\dot{\mathbf{r}}_{C2}\right)\frac{\dot{\mathbf{r}}_{C1}}{[\dot{\mathbf{r}}_{C1}]} + \left(\frac{1}{2}\rho_{air}A_{2R}C_{2R}\mathbf{v}_{wind}{}^{T}\mathbf{v}_{wind}\right) \tag{39}$$

where A_{1R} and A_{2R} are the frontal areas of the first and second bodies, respectively, and C_{1R} and C_{2R} are the aerodynamic coefficients of bodies. ρ_{air} is the air density, and $\mathbf{v}_{wind}$ is the vector of wind speed. General system of equations of the container spreader and lifting mechanism can be written as

$$\dot{\mathbf{x}}(t) = \{f(\mathbf{x}(t), \mathbf{u}(t), \mathbf{d}(t))\} \tag{40}$$

Here, $\mathbf{d}(t)$ is the vector of the excitation and disturbance forces (wind and other factors), and $\mathbf{x}(t)$ is the vector of dynamic system state

$$\mathbf{x}(t) = \left\{\begin{array}{l} M_{e1}, M_{e2}, M_{e3}, \varphi_{11}, \varphi_{12}, \varphi_{13}, \varphi_{14}, \varphi_3, \varphi_4, \mathbf{r}_{C1} \\ \varphi_1, \mathbf{r}_{C2}, \varphi_2, \varphi_{21}, \varphi_{22}, \dot{\varphi}_{11}, \dot{\varphi}_{12}, \dot{\varphi}_{13}, \dot{\varphi}_{14} \\ \dot{\varphi}_3, \dot{\varphi}_4, \dot{\mathbf{r}}_{C1}, \varphi_1, \dot{\mathbf{r}}_{C2}, \dot{\varphi}_2, \dot{\varphi}_{21}, \dot{\varphi}_{22} \end{array}\right\} \tag{41}$$

$\mathbf{u}(t)$ is the action vector

$$\mathbf{u}(t) = \{U_{rede1}, U_{rede2}, U_{rede3}\}^T \tag{42}$$

In the next section, the results of multibody dynamic simulation are presented.

Simulation results and discussions

The simulation of the container spreader and lifting mechanism will help detect motion deviations of the quay crane in real time. The mathematical model was developed for scaled quay crane prototype as shown in the previous section. Any crane's control algorithm optimization was not included in the simulation. In the mathematical experiment, the vibrations were simulated during the transient processes. The main target of the simulation was to calculate the influence of the transient processes for quay crane model. The cargo lifting process was simulated for the first and second motors.

The initial values of the model parameters used for the mathematical experiment are presented in Table 1. The duration of simulation was 10 s, but the transient motions stabilize after about 2 s and most of the represented results are in this time period.

The graphs of the angular velocity of the first and second motors with the pulleys are presented in Figure 4. This is a standard transient process of the asynchronous motor. The transient processes of both the motors last for 0.2 s as shown in Figure 4. The motor's pulley's transient lasts longer—about 1.0 s. These simulation results show that both the motors in the crane system work similar.

The motors also have an impact on the cargo lifting speed due to the transient processes. As shown in Figure 5, high-amplitude vibrations affect the vertical velocities of cargo lifting. These vibrations last longer than motor transient process, because the container is suspended and the cables are tensioned by cargo weight. As shown in Figure 5, the transient process lasts about 1.4 s.

The cargo displacements are shown in Figure 6. There are two components (coordinates by Y- and Z-axis) of vector $\mathbf{r}_{C2}$. The cargo horizontal displacement

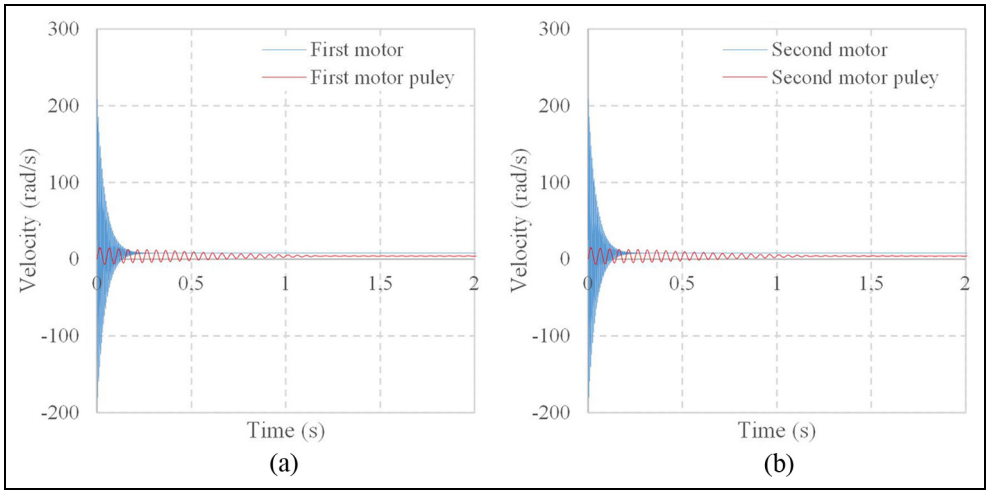

Figure 4. Angular velocities of motor and pulley: (a) first motor with pulley and (b) second motor with pulley.

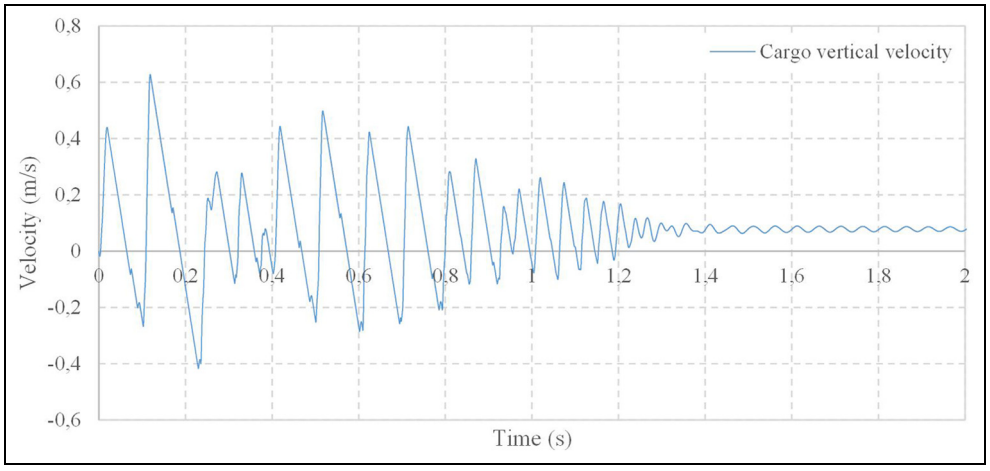

Figure 5. Vertical velocities of cargo lifting.

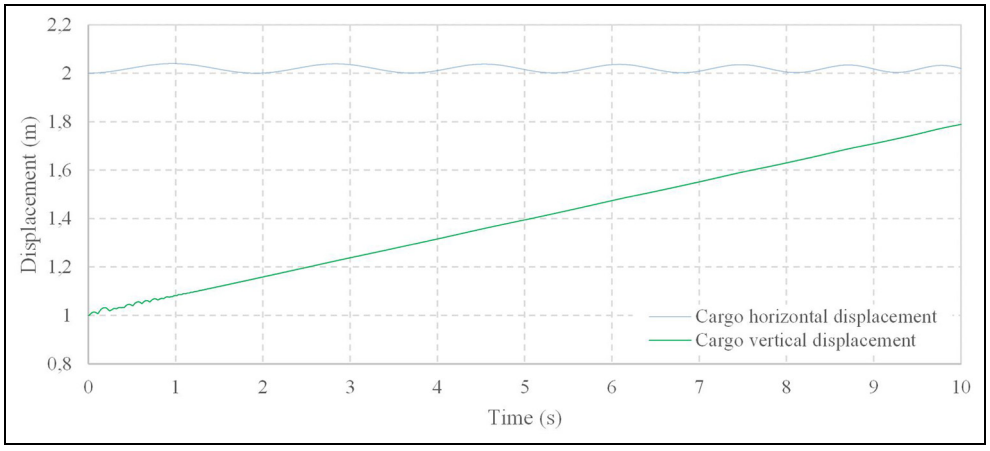

Figure 6. Cargo horizontal (by *Y*-axis) and vertical (by *Z*-axis) displacements.

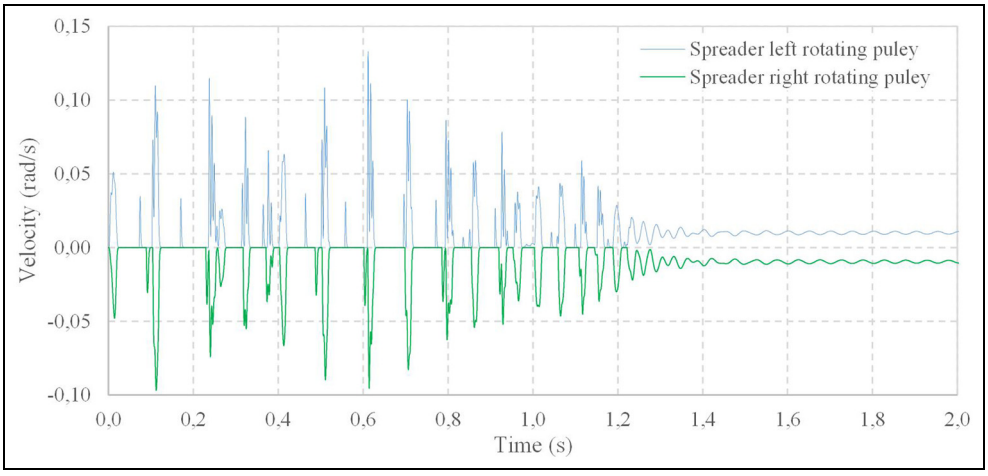

Figure 7. Velocities of left and right rotating pulleys on spreader.

(by Y-axis) shows the sway, where the amplitude is about 5 cm. The vertical displacement (by Z-axis) shows the coordinate of cargo lifting. The estimated cargo lifting speed is 0.08 m/s. During the simulation, the cargo is lifted up to 0.8 m (from 1 to 1.8 m) in 10 s.

In Figure 7, the angular velocities of the pulleys of the spreader are presented. Both the pulleys rotate at the same speed but in opposite direction. The right pulley rotates clockwise and left anticlockwise. During the lifting process, both the pulleys rotate at low angular velocities and the transient process lasts about 1.4 s. As it is shown in Figure 8, after the transient behavior of the rotating pulleys, the angular velocity is about 0.01 rad/s. The pulleys on the spreader are affected by friction. This leads to excessive vibrations during the transient. The simulation results presented in Figures 6 and 7 show even lift of the cargo.

During the simulation of container lifting, the motors' transient processes affect the whole crane system. This influence is presented in Figure 8. Although the trolley is stationary, the transient process spreads vibration to all axes. In Figure 8(a) and (c), the horizontal and vertical trolley velocities are shown. This transient process lasts about 1.5 s and after the transient behavior, the velocity becomes equal to 0 (stabilizes dynamic balance of the trolley). In Figure 8(b) and (d) the phase space diagrams of the reciprocating motion of the horizontal and vertical displacements are presented. These phase space diagrams show the maximum displacements of the trolley, minimal, and maximal velocities. Also, the dynamic balance of the trolley stabilizes and the displacement becomes equal to 0. It happens because a cargo is lifted at a constant speed.

The performed multibody dynamics simulation of the container spreader and lifting mechanism shows that vibrations affect the whole system. Typical transient of asynchronous motor caused vibrations during system startup.[16,17] These vibrations induced by motors show that the developed dynamics model and its simulation results can be applied to future research to solve predictive control problems.

Conclusion

In this article, a multibody, more accurate mathematical model was designed to investigate the transients of the quay crane trolley and spreader on the quay crane system startup. The dynamics simulation was performed for the vertical crane spreader travel to imitate the container vertical motion and its influence for cargo sway and trolley displacements when the trolley motor is not running. The simulation results were obtained and investigated. According to the simulation results, in all the cases, the transients induced by startup of the vertical spreader travel affect the whole crane system. Due to the influence of flexible cable, lifting of the spreader causes oscillations which results in additional sway of cargo and reciprocating trolley displacement. These transient processes affect the whole system of the crane and last from 0.2 s at motors to 1.4 s at rotating pulleys on the spreader because the mathematical model includes flexible cables. The pulley–flexible cable system prolongs transients approximately seven times. The maximum vertical displacement ($68 \cdot 10^{-5}$) of the trolley is 42 times higher than the horizontal displacement ($1,6 \cdot 10^{-5}$). As a result, the spreader stabilizes after 2 s from crane system startup.

The developed mathematical model of the intermodal crane spreader can be used for real size crane transportation process imitation, but some parameters have to be adjusted. In addition, this mathematical model could be improved by adding additional functions and used as tool for crane control algorithm verification and detection of weak points in similar systems. This will help to improve safety in cargo transportation process by including transient-induced vibration

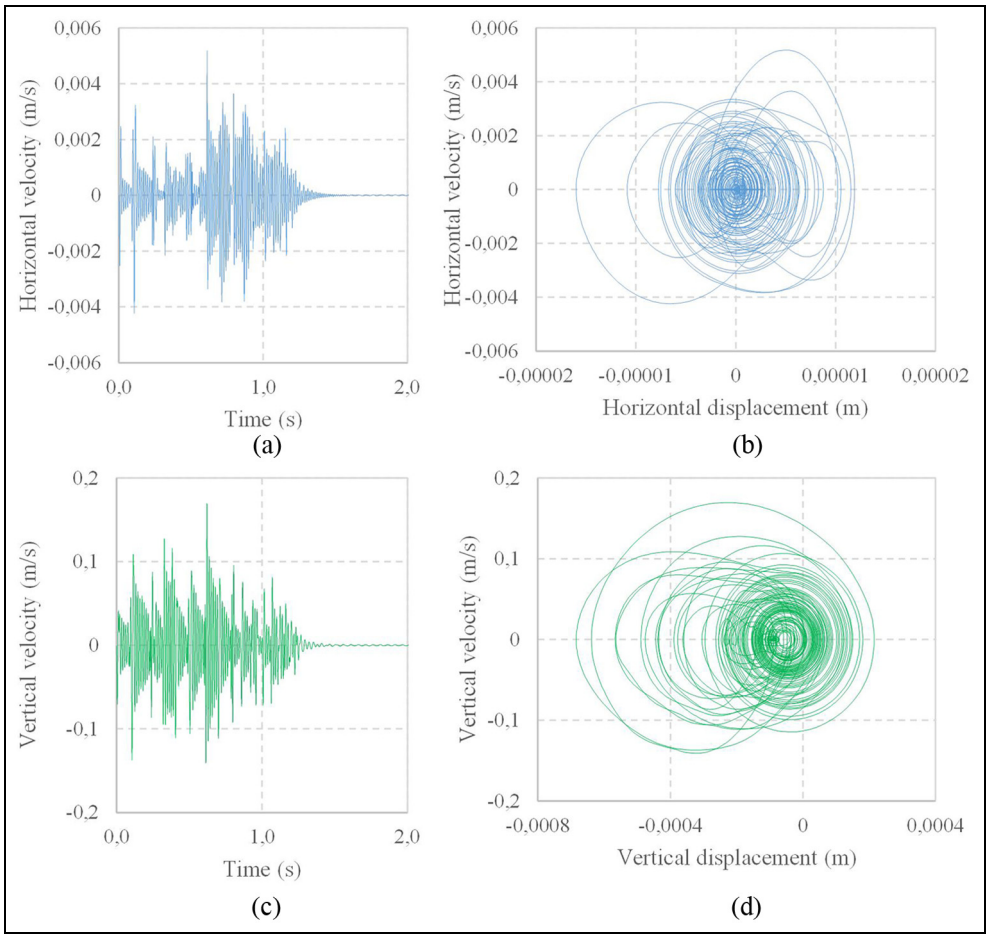

Figure 8. Trolley vibrations: (a) horizontal velocity of trolley, (b) phase space diagram of reciprocating motion horizontal displacement, and (c) vertical velocity of trolley, and (d) phase space diagram of reciprocating motion vertical displacement.

information to quay crane control algorithm as container additional sway compensator.

Acknowledgement

Author Marijonas Bogdevicius is also affiliated with Marine Science and Technology Centre, Klaipeda University, Klaipeda, Lithuania.

Declaration of conflicting interests

The author(s) declared no potential conflicts of interest with respect to the research, authorship, and/or publication of this article.

Funding

The author(s) received no financial support for the research, authorship, and/or publication of this article.

References

1. Roso V, Woxenius J and Lumsden K. The dry port concept: connecting container seaports with the hinterland. *J Transp Geogr* 2009; 17: 338–345.
2. Kawai H, Choi Y, Kim YB, et al. Position measurement of container crane spreader using an image sensor system for anti-sway controllers. In: *Proceedings of the international conference control, automation and systems*, Seoul, South Korea, 14–17 October 2008, pp.683–686. New York: IEEE.
3. Chang C-H, Xu J and Song D-P. An analysis of safety and security risks in container shipping operations: a case study of Taiwan. *Safety Sci* 2014; 63: 168–178.
4. Hellendoorn H, Mulder S and De Schutter B. Hybrid control of container cranes. In: *Proceedings of the IFAC proceedings volumes*, vol. 44, January 2011, pp.9697–9702. Elsevier, http://www.sciencedirect.com/science/article/pii/S1474667016451694
5. Ahmad MA, Saealal MS, Zawawi MA, et al. Classical angular tracking and intelligent anti-sway control for rotary crane system. In: *Proceedings of the international conference on electrical, control and computer engineering 2011 (InECCE)*, Kuantan, Malaysia, 21–22 June 2011, pp.82–87. New York: IEEE.
6. Cao L and Liu L. Adaptive fuzzy sliding mode method-based position and anti-swing control for overhead cranes. In: *Proceedings of the 2011 third international conference measuring technology and mechatronics automation*, Shanghai, China, 6–7 January 2011, pp.335–338. New York.

7. Yoshihara H, Fujioka N and Kasahara H. A new vision-sensorless anti-sway control system for container cranes. In: *Proceedings of the 38th IAS annual meeting conference record of the industry applications conference*, Salt Lake City, UT, 12–16 October 2003, vol. 1, pp.262–269. New York: IEEE.
8. Nundrakwang S, Benjanarasuth T, Ngamwiwit J, et al. Multivariable control of overhead crane system by CRA method. In: *Proceedings of the 2008 SICE annual conference*, Tokyo, Japan, 20–22 August 2008, vol. 1, pp.3278–3282. New York: IEEE.
9. Jaafar HI, Mohamed Z, Jamian JJ, et al. Dynamic behaviour of a nonlinear gantry crane system. *Proced Technol* 2013; 11: 419–425.
10. Ismail RMTR, Ahmad MA, Ramli MS, et al. Nonlinear dynamic modelling and analysis of a 3-D overhead gantry crane system with payload variation. In: *Proceedings of the 2009 third UKSim European symposium on computer modeling and simulation*, Athens, 25–27 November 2009, pp.350–354. New York: IEEE.
11. Bogdevicius M and Vika A. Investigation of the dynamics of the overhead crane lifting process in the vertical plane. *Transp* 2005; 20: 176–180.
12. Tomczyk J, Cink J and Kosucki A. Dynamics of an overhead crane under a wind disturbance condition. *Automat Constr* 2014; 42: 100–111.
13. Cha J-H, Roh M-I and Lee K-Y. Dynamic response simulation of a heavy cargo suspended by a floating crane based on multibody system dynamics. *Ocean Eng* 2010; 37: 1273–1291.
14. Wu T-S, Karkoub M, Yu W-S, et al. Anti-sway tracking control of tower cranes with delayed uncertainty using a robust adaptive fuzzy control. *Fuzzy Set Syst* 2016; 290: 118–137.
15. Qian D, Tong S and Lee S. Fuzzy-logic-based control of payloads subjected to double-pendulum motion in overhead cranes. *Automat Constr* 2016; 65: 133–143.
16. Sarac V and Cvetkovski G. Transient analysis of induction motor using different simulation models. *Acta Tech Jaurinensis* 2013; 6: 65–75.
17. Slater RD, Sc B, Wood WS, et al. Constant-speed solutions applied to the evaluation of induction-motor transient torque peaks. *Inst Electr Eng* 1967; 114: 1429–1435.